Biological and Biomedical Journal

Journal homepage: https://bbj.journals.ekb.eg

Histological and immunohistochemical study of the effect of sofosbuvir and its withdrawal on the submandibular salivary glands and tongue of adult male albino rats

Shimaa M. Badr*, Eman M. El-Beltagi, Suzan Elsayed Abo Elnasr

Histology and Cell Biology, Faculty of Medicine,Tanta University, Egypt.

ARTICLE INFO

Received: 1/10/2024

Accepted: 23/10/2024

Corresponding author:

Shimaa M. Badr, Ph. D

Shaimaa.badr@med.tanta.edu.eg

Mobile: (+2) 01142052244

P-ISSN: 2974-4334

E-ISSN: 2974-4324

DOI:

10.21608/bbj.2024.325405.1045

ABSTRACT

Hepatitis C virus (HCV) infection has been considered a core reason of chronic liver disorder. Sofosbuvir (SOF) is part of a combined antiviral therapy regimen used to treat chronic HCV infection associated with many side effects. The aim of the study is to demonstrate the effect of SOF and its withdrawal on the submandibular salivary gland as well as on the tongue of adult male albino rats. Thirty adult male albino wistar rats were included in this work. They were randomly split into three groups: group I was the control group. Group II received SOF at a dose of 41 mg/kg once daily orally for four weeks. Group III received SOF as group II and then were kept without treatment for another four weeks. Submandibular glands and tongue samples were processed histologically and immunohistochemically. Morphometrical and statistical studies were implemented. Group II (SOF-treated group) submandibular gland sections revealed marked histological alterations at both ductal and acinar levels. Tongue specimens of this group also showed marked affection of filiform papillae, which was confirmed by scanning electron microscopy. A highly significant rise in the mean area percentage of collagen fibers as well as a highly significant decline in the area percentage of E-cadherin were evident in group II versus the control group at both submandibular glands and tongue specimens. Most changes were ameliorated in the withdrawal group (GIII). In conclusion SOF induces structural changes in submandibular salivary glands and tongue which decreased after its withdrawal.

Key words: Sofosbuvir, Tongue, Submandibular salivary glands, E-cadherin

1. Introduction

Hepatitis C virus (HCV) infection is one of the public health troubles in Egypt (Elkashef et al., 2022). It is typically asymptomatic but hepatocellular carcinoma (HCC) and cirrhosis are two major consequences of chronic HCV infection, with 20% of cases developing HCC (Henriot et al., 2022). Pegylated interferon injections with daily ribavirin were the standard therapy for treating HCV infection. This treatment plan was costly, difficult to administer, and had a less than 50% cure rate, particularly for cirrhotic patients (El-Ghitany, 2019). In 2014, Egypt started a vigorous screening and treatment plan, and eventually developed into a nationwide strategy to end the threat of HCV to public health by 2021(Hassanin et al., 2021). This protocol included a daily sofosbuvir (SOF) and any other direct-acting antiviral agents. As compared to formerly applied treatments, SOF-dependent regimens provided a better cure rate (>90%), and

a two- to fourfold shortening in the period of remedy (Ibrahim et al., 2021). SOF (known traditionally as Sovaldi) is a nucleotide analogue NS5B polymerase inhibitor that was actually accepted by the Food and Drug Administration in 2013 (Cha and Budovich, 2014). SOF active metabolite does not inhibit human DNA or RNA polymerases or mitochondrial RNA polymerases (Ali et al., 2024). Many side effects were recorded due to SOF administration such as nausea, vomiting, and diarrhea in addition to oral ulcers and sores. Furthermore, dyspepsia, abdominal discomfort, gastroesophageal reflux and constipation were recorded (El-ghazouly and Yassien, 2022). Moreover, some histopathological changes of many organs as stomach, testes, kidney and brain were reported following SOF administration (El-Kholy et al., 2019; Ibrahim et al., 2020; Mohamed et al., 2021) . Dry mouth or xerostomia is also one of the reported side effects following SOF administration (El-ghazouly and Yassien, 2022). Daniel et al. (2000) reported that xerostomia could be caused by salivary gland hypofunction and diagnosed by fissured tongue or atrophy of tongue papillae. Therefore, this work was constructed to demonstrate the effect of SOF as well as its withdrawal on the submandibular salivary glands and the tongue of adult male albino rats.

2. Materials and methods

Drugs

Sofosbuvir was purchased from Marcyrl Pharmaceutical Industries, El Obour City, Egypt. It was available under the trade name (Mpiviropack) in tablet form which was dissolved in distilled water. The administered dose in this study was 41 mg/kg orally once daily for 4 weeks (El-Kholy et al., 2019).

Animals

Thirty adult male albino wistar rats aged 3 months of an average weight of 180–200 grams were included. The animals were stayed for one week before starting the experiment to allow for adaptation. The experimental design and handling procedures were performed consistent with the guidelines of the Local Ethical Committee of the Faculty of Medicine, Tanta University, Egypt (Approval number: 36264PR582/2/24).

Experimental design

The rats were divided in a random manner into three main groups (10 rats each) as follows: Control group (G I): included 10 rats and were subdivided into: Subgroup-A: It comprised of 5 rats that were kept without any treatment. Subgroup-B: It comprised of 5 rats that received 1 ml of distilled water once daily orally for four weeks. SOF-treated group (G II): It comprised of 10 rats that were given SOF at a dose of 41 mg/kg once daily orally via a gastric tube for four weeks dissolved in 1 ml distilled water (El-Kholy et al., 2019). Withdrawal group (G III): It comprised of 10 rats that were given SOF at the same dose, manner and period as group II then, they were kept without any treatment for another four weeks for the possibility of recovery.

The day after the last dose, all rats were anesthetized by sodium pentobarbital (Ghasi et al., 2020). Then, the submandibular salivary gland samples were dissected and prepared for light microscopic examination. Tongue samples were also dissected from the oral cavity of all animals to be prepared for light and scanning electron microscopic examination. In accordance with safety protocols and infection control procedures, the bodies of slaughtered animals were shipped with the hospital's biohazards in special packaging.

Processing for light microscopy

The submandibular salivary gland and tongue specimens (apex and body) were prepared and stained with hematoxylin and eosin (H&E) and masson's trichrome according to (Bancroft and Layton, 2019a; Bancroft and Layton, 2019b)

Immunohistochemical staining for E-Cadherin Expression in Submandibular Salivary Glands and Tongue Sections

E-cadherin is a transmembrane protein that plays a crucial role in cell adhesion and functional integrity, particularly in epithelial tissues **(**Sisto et al., 2022)**.** Submandibular salivary glands and tongue sections (5-µm thick) were deparaffinized and hydrated. Antigen retrieval of deparaffinized sections was done by immersing the sections in a preheated citrate buffer solution (pH=6) and maintaining heat in a microwave at 121˚C for 5-

10 minutes. Then, endogenous peroxidase activity was blocked and washed in phosphate buffered saline. After that, the slides were incubated with diluted 1:100 primary anti-E-cadherin antibody (Rabbit, polyclonal, Santa Cruz Biotechnology, USA) at 4°C overnight in a humidified chamber. The sections were then immersed in PBS and consequently incubated with biotinylated goat secondary antibodies for 30 minutes. Diaminobenzidine tetrahydrochloride (DAB) solution (Sigma–Aldrich, Darmstadt, Germany) was applied as a chromogen and hematoxylin was used as a counterstain, then dehydrated and cover slipped. Negative control sections were prepared by the similar preceding steps without adding the primary antibody. The positive reaction was identified as brownish membranous deposits in the serous as well as ductal cells of the submandibular salivary gland and the epithelial cells of the tongue (Essawy et al., 2021; Kandeel and Elwan, 2023). The positive control for E-cadherin was the colon (Fig. 1). All slides were assessed and photographed using a light microscope (Olympus, Japan) with a built- in camera at the Histology and Cell Biology Department, Faculty of Medicine, Tanta University, Egypt.

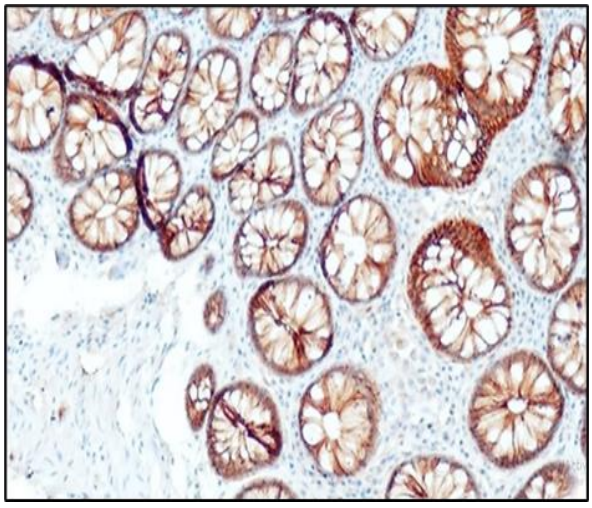

Fig. 1. A colon section as a positive control for E-cadherin immunostaining.

Morphometric study

The image J software (version 1.48v National Institute of Health, Bethesda, Maryland, USA) was used for image analysis. Ten photos from each group were examined and analyzed to quantify: The mean height of the filiform papillae on the dorsal mucosal surface of the tongue at a magnification x200 in H&E-stained tongue specimens (Shalaby and Kashef, 2021). The Mean epithelial thickness of the ventral mucosal surface of the tongue was measured at a magnification x200in H&E-stained tongue specimens (Shalaby and Kashef, 2021). The mean area percentage of collagen fiber in Masson's trichrome stained sections at a magnification x200 for submandibular salivary gland specimens and at a magnification x100 for tongue specimens (El-ghazouly and Yassien, 2022). The mean area percentage of E-cadherin in immunohistochemically stained sections at a magnification x400 (Hosny et al., 2020) for both salivary gland and tongue specimens.

Processing for scanning electron microscopy

Specimens from the tongues were fixed in 2.5% glutaraldehyde and post-fixed in 1% osmium tetroxide, then dehydrated in serial dilutions of ethanol and placed into amyl acetate. After being dried with liquid CO2, the samples were covered in gold (Rau et al., 2001). The dorsal surfaces of the tongue samples were examined under a JEOL JSM-5200LV scanning electron microscope at the Electron Microscope Unit, Faculty of Medicine, Tanta University, Egypt.

Statistical analysis

One-way analysis of variance (ANOVA) was used to analyze the morphometric results then the Tukey's post hoc test was done. Differences were reflected as statistically significant if the probability value $p<0.05$ and highly significant if $p<0.001$, while $p>0.05$ was reflected as statistically insignificant.

3. Results

A-Submandibular salivary glands

H&E-stained sections

In control group (GI), the submandibular gland sections exhibited a normal histological structure. The gland was composed of multiple lobules separated by thin interlobular connective tissue septa that appeared to transmit the blood vessels and interlobular excretory ducts lined by stratified columnar epithelium. Each lobule was composed of densely packed serous acini and intralobular ducts such as the intercalated ducts, striated ducts, and granular convoluted ducts

(Fig. 2a). The serous cells seemed pyramidal with basophilic cytoplasm and spherical basally located nuclei. The intercalated ducts were lined by short simple cuboidal epithelium while the lining epithelium of the striated ducts was simple columnar epithelium with oval to spherical centrally located nuclei and deeply stained acidophilic cytoplasm illustrating basal striations. Meanwhile, the granular convoluted ducts were lined by high simple columnar epithelium with large spherical basally located nuclei and acidophilic cytoplasm showing apical acidophilic secretory granules (Fig. 2b). In addition to the serous acini, the lobules contained mucous acini with flattened dark nuclei and foamy pale-stained cytoplasm. Some of these mucous acini were capped by a serous demilune (Fig. 2c). Examination of the gland sections of SOF-treated group (GII) revealed marked structural changes. The gland lobules showed disturbed architecture at both the acinar and ductal levels. Some lobules revealed shrunken disorganized acini and irregular outlined ducts with peri-acinar and peri-ductular inflammatory cellular infiltration (Fig. 3a). Other lobules exhibited widened spaces between the acini and the ducts with extravasated blood in-between (Fig. 3b).

At the cellular level, the serous acinar cells showed nuclei compressed by cytoplasmic vacuoles with diminished cytoplasmic basophilia. Other cells exhibited ill-defined karyolytic fading nuclei (Fig. 3b-d). Concerning the intralobular ducts, the intercalated ducts appeared disorganized with irregular nuclei. The striated ducts were disorganized with cytoplasmic vacuoles and dark nuclei of their lining epithelium. Moreover, focal loss of the basal striations, in addition to stagnant secretion with epithelial sloughing into the lumina of some striated ducts were observed. Furthermore, the granular convoluted ducts showed diminished acidophilic cytoplasmic granules. Their lining cells exhibited vacuolated cytoplasm and dark irregular nuclei. Moreover, discontinuous and focally detached basement membranes of some disorganized ducts were observed **(**Fig. 3b&d**).** On the other side, the interlobular connective tissue septa appeared thickened with marked fibrosis, infiltration of inflammatory cells, and dilated congested blood vessels. The excretory ducts illustrated stagnant secretion inside their lumina (Fig. 3e). Other ducts showed sloughing of some epithelial lining cells into the lumen with widened intercellular spacing (Fig. 3f). No changes were observed as regards the mucous acini. Regarding Withdrawal group (GIII), examination of sections from this group revealed more or less partial improvement and restoration of the structure of the submandibular salivary gland. The gland appeared divided into lobules separated by interlobular connective tissue septa with mild inflammatory cellular infiltration. The lobules of the gland contained more or less closely packed serous acini and intralobular ducts (Fig. 4 a). The serous acini and ducts were more or less normal with the exception of some cells having cytoplasmic vacuoles and dark nuclei (Fig. 4b-c).

Masson's trichrome-stained sections

Submandibular gland sections of control group (GI) depicted fine scanty collagen fibers in the interlobular connective tissue septa around the blood vessels and large excretory ducts and around the intralobular ducts and acini (Fig. 5 a). SOF-treated group (GII) showed apparently increased collagen fibers in the interlobular connective tissue septa extending to surround the intralobular ducts and acini (Fig. 5 b). Meanwhile, withdrawal group (GIII) revealed an apparently moderate amount of collagen fibers in the interlobular connective tissue septa and around the intralobular ducts and acini (Fig. 5 c). Statistically, a highly significant rise in the mean area percentage of collagen was displayed in GII (45.03±0.92) (p<0.001) versus GI (5.72±1.61). However, GIII (7.70±0.85) exhibited a non-significant difference (p>0.05) compared to GI (Fig. 5 d).

E-cadherin immunohistochemically stained sections

A negative control section of the submandibular gland was illustrated (Fig. 6 a). Control group (GI) revealed an apparent strong positive membranous reaction in the acini and ducts of the submandibular glands (Fig. 6 b). SOF-treated group (GII) revealed an apparent weak positive membranous reaction in the majority of acini and ducts (Fig. 6 c). However, Withdrawal group (GIII) revealed an apparent strong positive membranous reaction in the majority of acini and

ducts (Fig. 6d). Statistically, a highly significant decline in the mean area percentage of E-cadherin immunoexpression was illustrated in GII (1.81±0.54) (p<0.001) versus GI (6.37±0.62) whereas, GIII (5.55±0.31) revealed a non-significant difference (p>0.05) as compared to GI (Fig. 6 e).

B-Tongue H&E--stained sections

Concerning the tongue sections of control group (GI), the anterior 2/3 of the dorsal surface of the tongue showed characteristic projections, the lingual papillae. The filiform type of papillae, which had regular organization, orientation, and a conical shape with tapering tips, were the most common (Fig. 7 a and b). The mushroom-shaped fungiform papillae with taste buds on their upper surface that were barrel in shape, were less numerous and dispersed among the filiform ones (Fig. 7 c). Each lingual papilla was formed of a covering epithelium and a core formed of loose connective tissue having blood vessels. Regarding the epithelium, it was a stratified squamous keratinized epithelium lying on a basement membrane with many epithelial ridges (Fig. 7 b and c). Meanwhile, the mucosa covering the ventral surface was composed of a stratified squamous epithelium with a keratin layer and lamina propria formed of loose connective tissue containing small blood vessels (Fig. 7 d). Lingual muscles arranged in different directions were also observed (Fig. 7 a and d).

Meanwhile, tongue sections of SOF-treated group (GII) depicted alterations in the histological structure. On the dorsal surface, there was a focal disappearance of the filiform papillae as well as disorganized fungiform papillae (Fig. 8a). A noticeable decline in the height of the filiform papillae, that was represented as statistically highly significant (327.29±15.00) (p<0.001) as compared to control group (528.93±16.63) and some with blunted ends were observed. Additionally, focal discontinuity of the keratin layer was also observed. The covering epithelial cells showed vacuolation of the cytoplasm and dark nuclei as well as an apparent decrease in the epithelial layers and focal absence of the papillary ridges. In addition, inflammatory cellular infiltration was observed in the connective tissue core (Fig. 8 b-e). Regarding the ventral surface, apparent thinning of the covering epithelial cells, that was represented as statistically highly significant (72.28±20.81) (p < 0.001) as compared to control group (257.71±24.29), with focal separation of the keratin layer was noticed. Additionally, dilated blood vessels were present in the lamina propria (Fig. 8 f and g).

The withdrawal group (GIII) showed that on the dorsal surface of the tongue, most of the filiform papillae were shown with normal shape, distribution and height that was represented as statistically highly significant increase (463.01±69.25) (p<0.001) as compared to GII and non-significant difference (p>0.05) as compared to control group. A few filiform papillae appeared with blunted ends (Fig. 9 a). Additionally, a nearly normal fungiform papilla with a taste bud on its upper surface was also observed (Fig. 9 b). Regarding the ventral surface, nearly normal covering epithelium that restored its thickness as statistically highly significant increase (226.49±18.07) (p<0.001) as compared to GII and non-significant difference (p>0.05) as compared to control group. and lamina propria were noticed (Fig. 9 c). The histogram representing the mean height of the filiform papillae and mean epithelial thickness of the ventral mucosal surface of the tongue of the different studied groups was illustrated in (Fig. 10).

Masson's trichrome-stained sections

Examination of the tongue sections obtained from control group (GI) showed fine collagen fibers in the connective tissue core of the dorsal surface as well as in the lamina propria of the ventral surface (Fig. 11 a and b). Concerning SOF-treated group (GII), there was an apparent rise in the collagen fibers deposition in the connective tissue core of the dorsal surface papillae and in the lamina propria of the ventral surface (Fig. 11c and d). However, the Withdrawal group (GIII) revealed an apparently moderate amount of collagen fibers in the connective tissue core of the dorsal surface papillae and in the lamina propria of the ventral surface (Fig. 11e and f). Statistically, a highly

significant rise in the mean area percentage of collagen in dorsal and ventral tongue surfaces was displayed in GII (13.47±3.47, 12±1.61 respectively) (p<0.001) versus GI (3.78±0.86, 3.09±0.86 respectively). However, GIII (5.02±0.62, 4.37±0.68 respectively) exhibited a non-significant difference (p>0.05) compared to G I (Fig. 11 g).

E-cadherin immunohistochemically stained sections

Negative control sections of the tongue were illustrated (Fig. 12 a and b). Examination of E-cadherin tongue sections obtained from Control group (GI) showed an apparent strong positive membranous reaction in almost all layers of the epithelium of both dorsal and ventral surfaces (Fig. 12 c and d). As regards SOF-treated group (GII), there was an apparent weak positive membranous reaction in all epithelial layers at both dorsal and ventral surfaces. Statistically a highly significant decline in the mean area percentage of E-cadherin immunoexpression in dorsal and ventral tongue surfaces was illustrated in GII (1.16±0.88 and 0.67±0.49, respectively) (p<0.001) versus GI (8.55±1.77 and 4.23±1.1, respectively) (Fig. 12 e - f and i). Whereas withdrawal group (GIII) exhibited an apparent moderate positive membranous reaction in almost all layers of the epithelium with a non-significant difference (p>0.05) (7.84±2.4 and 4.05±0.48, respectively) versus GI (Fig. 12 g-h and i).

Scanning electron microscopic results

Examination of the dorsal surface of the tongue of the control group showed numerous filiform papillae with regular arrangement and shape. They were with conical tips that were directed in the same side. Moreover, scattered fungiform papillae having a taste pore in the center of its smooth upper surface were also observed (Fig. 13 a). Regarding the SOF-treated group, the following changes were observed. Irregularly arranged filiform papillae were observed. Some were thin and long, while others were short and atrophied with wide spaces between them. Irregular fungiform papillae were observed. Additionally, their upper surfaces were rough with ill-defined taste pore opening (Fig. 13 b-d). Concerning the withdrawal group, there was preservation of the morphological structure of the tongue papillae. Nearly normal filiform papillae with scattered fungiform papillae between them were observed (Fig. 13 e).

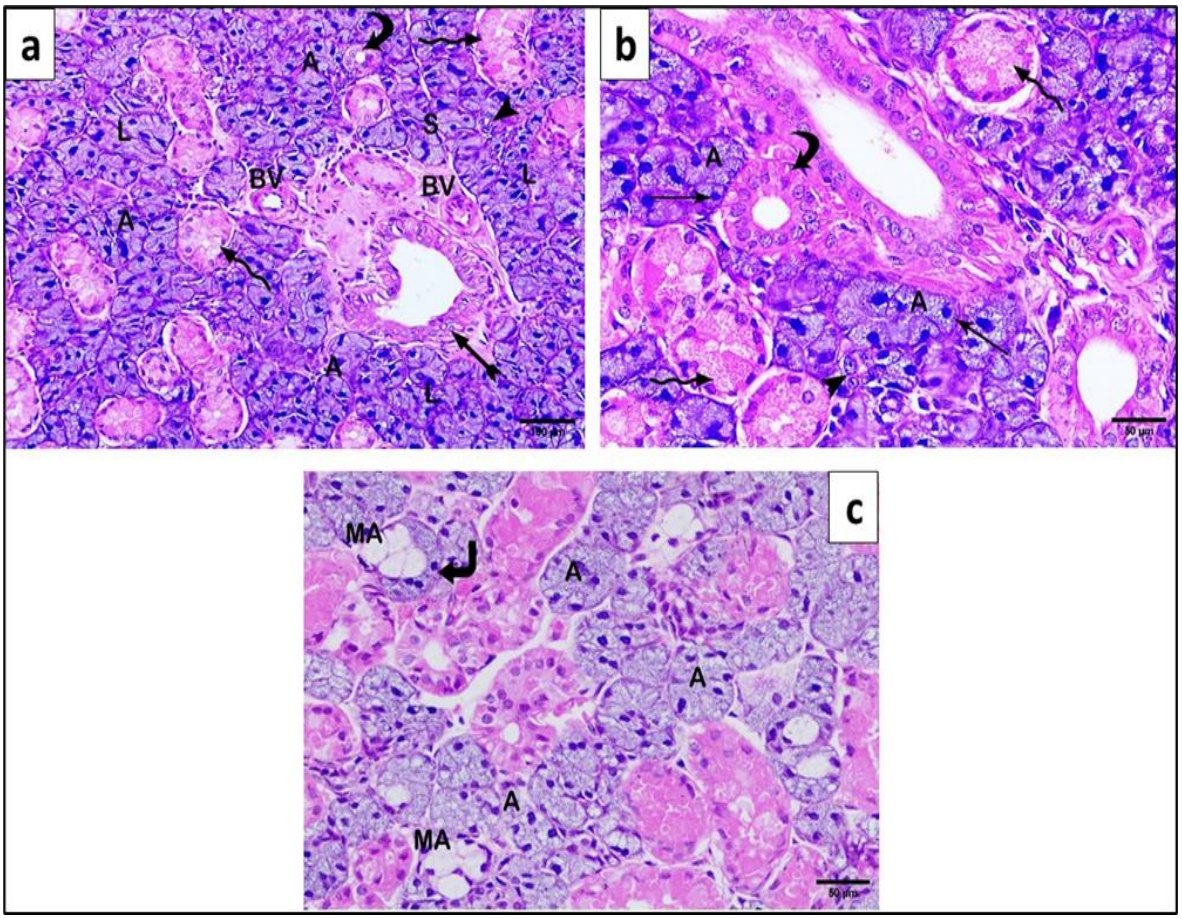

Fig. 2. Submandibular gland sections of control group (GI) showing: The gland is divided into lobules (L) separated by thin connective tissue septa (S) carrying the blood vessels (BV) and excretory ducts lined by stratified columnar epithelium (tailed arrow). Each lobule has serous acini (A) that are densely packed together and intercalated ducts (arrowhead), striated ducts (curved arrows) and granular convoluted ducts (wavy arrows). (b) Serous acinar cells (A) with darkly stained basophilic cytoplasm and spherical basal nuclei (arrows), intercalated ducts lined by short simple cuboidal epithelium (arrowhead), striated ducts lined by simple columnar cells having oval to rounded central nuclei and deeply stained acidophilic cytoplasm with basal striations (curved arrow) and granular convoluted ducts lined by high simple columnar epithelium having rounded basal nuclei and acidophilic cytoplasm with apical acidophilic secretory granules (wavy arrows) are observed. (c) Mucous acini (MA) are noticed in-between the serous acini (A). Some of them are capped by serous demilune (right-angled arrow) (H&E a x200 scale bar=100µ, b & c x400 scale bar =50µ).

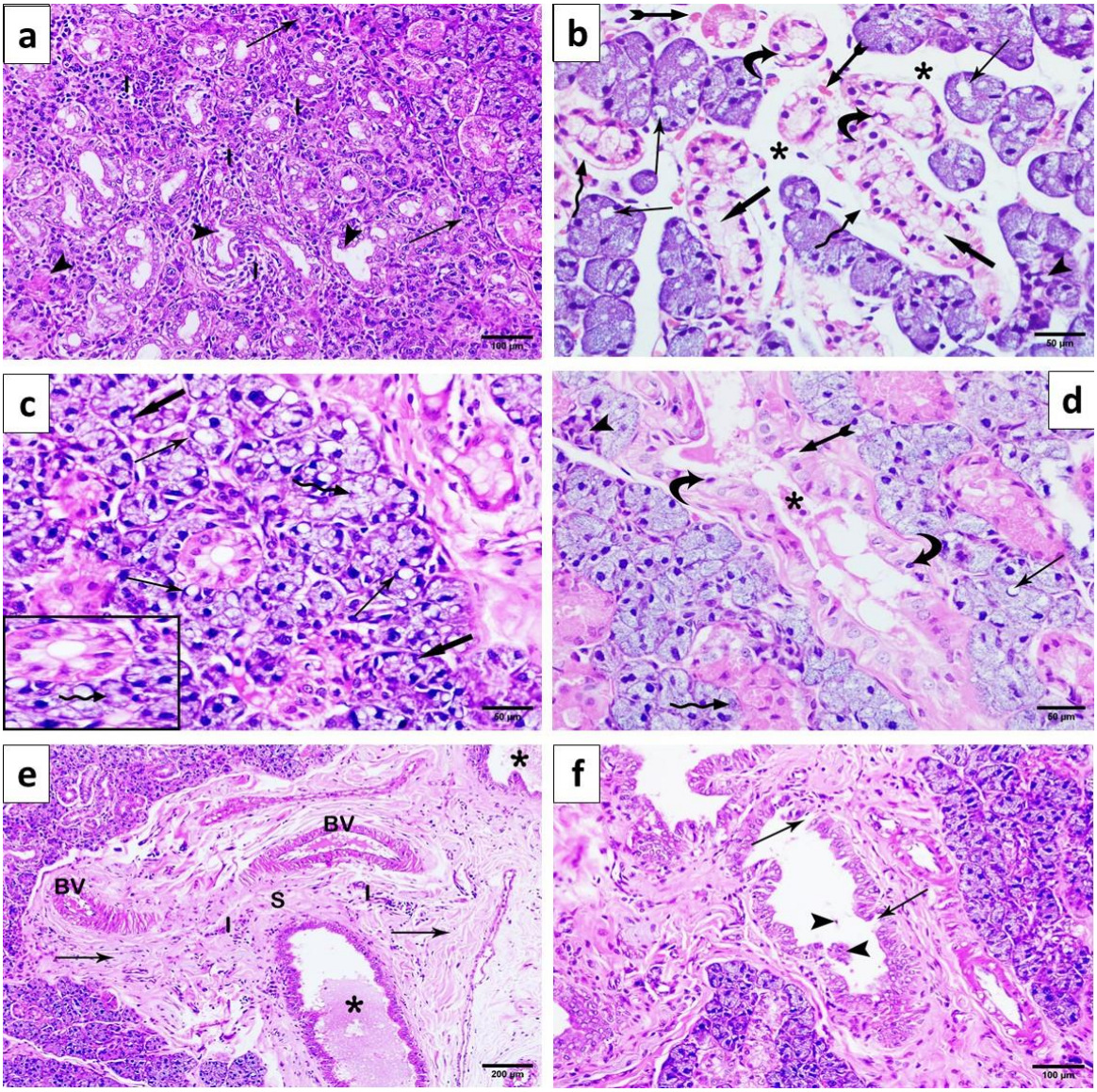

Fig. 3. Submandibular gland sections of SOF-treated group (GII) showing: (a) Shrunken disorganized acini (arrows) and irregular outlined ducts (arrow heads) with peri-acinar and peri-ductular inflammatory cellular infiltration (I) are noticed. (b) Widened spaces between the acini and the ducts (*) with extravasated blood in-between (tailed arrows). Serous acinar cells show nuclei compressed by cytoplasmic vacuoles (thin arrows). Intercalated ducts show vacuolated cytoplasm (arrowhead). Granular convoluted ducts appear with diminished acidophilic cytoplasmic granules (thick arrows), vacuolated cytoplasm and dark irregular nuclei (curved arrows). Discontinuous and focally detached basement membranes of some disorganized granular convoluted ducts are noticed (wavy arrows). (c) Serous acinar cells with nuclei compressed by cytoplasmic vacuoles with diminished cytoplasmic basophilia (arrows).Others appear with ill defined nuclei (wavy arrow) (d) Disorganized striated ducts with cytoplasmic vacuoles and dark nuclei of their lining epithelium (curved arrows). Focal loss of the basal striations (tailed arrow) and stagnant secretion with epithelial sloughing into the lumen (*) are observed. Disorganized intercalated duct with irregular nuclei (arrowhead) is noticed. Serous cells with nuclei compressed by vacuoles (arrow) or even fading nuclei (wavy arrow) are noticed. (e) Thick interlobular connective tissue septa (S) with marked fibrosis (arrows), inflammatory cellular infiltration (I) and dilated congested blood vessels (BV). ED shows stagnant secretion inside the lumen (*). (f) Excretory duct with sloughing of some epithelial lining cells into the lumen (arrow heads) and widened intercellular spacing (arrows) (H&E a x200 scale bar=100µ, b, c &d x400 scale bar =50µ, e x 100 scale bar= 200µ and f x200 scale bar=100µ).

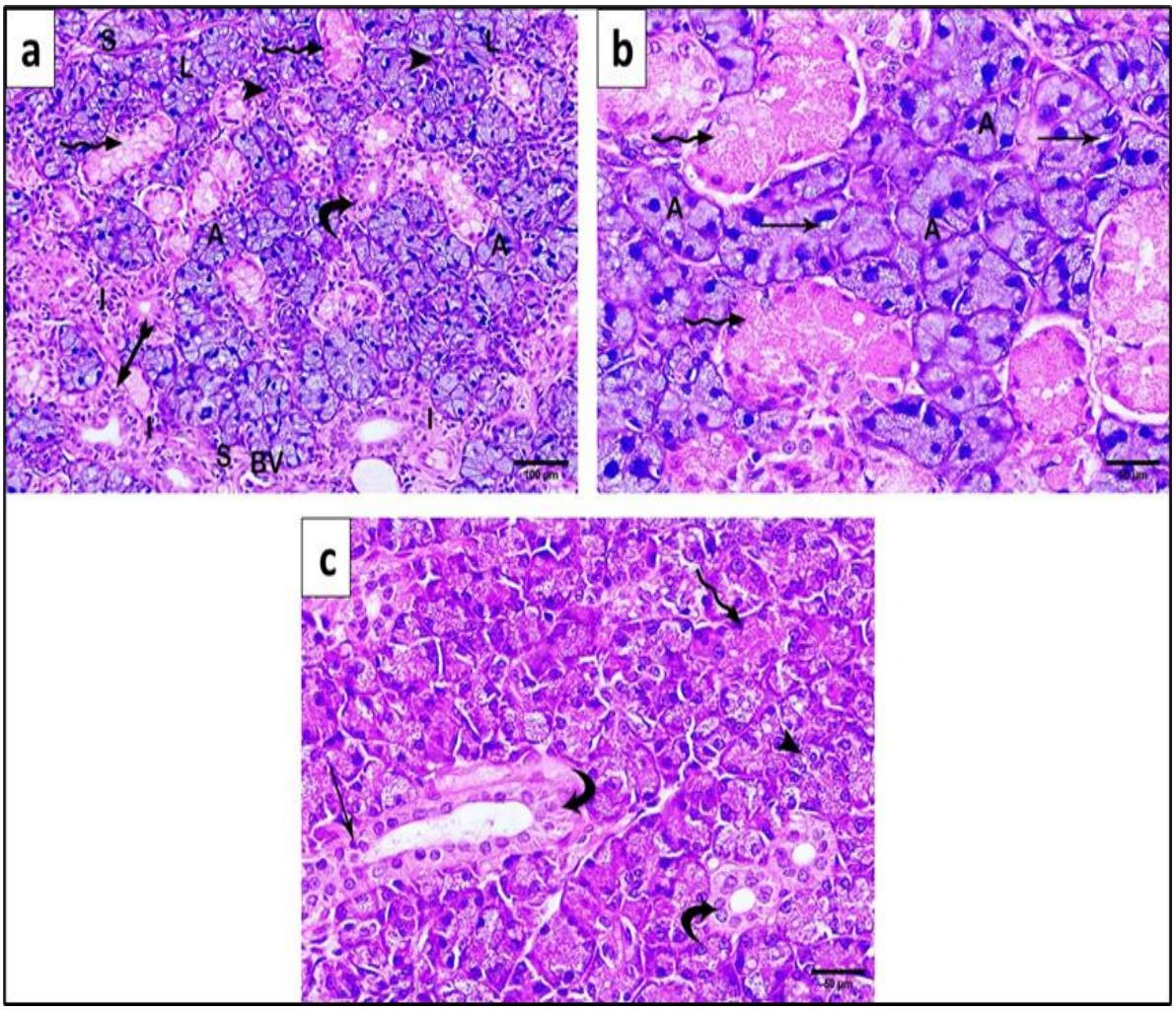

Fig. 4. Submandibular gland sections of withdrawal group (GIII) showing: (a, b and c) The gland is formed of lobules (L) with connective tissue septa (S) conveying the blood vessels (BV) between them and excretory ducts (tailed arrow). Each lobule contains closely packed serous acini (A), intercalated ducts (arrowhead), striated ducts (curved arrows) and granular convoluted ducts (wavy arrows). Mild inflammatory cellular infiltration (I) is noticed. (b) Few serous acinar cells show cytoplasmic vacuoles and dark nuclei (arrows). (c) Few lining cells of some striated ducts appear with dark nuclei (arrow) (H&E a x200 scale bar=100µ, b & c x400 scale bar =50µ).

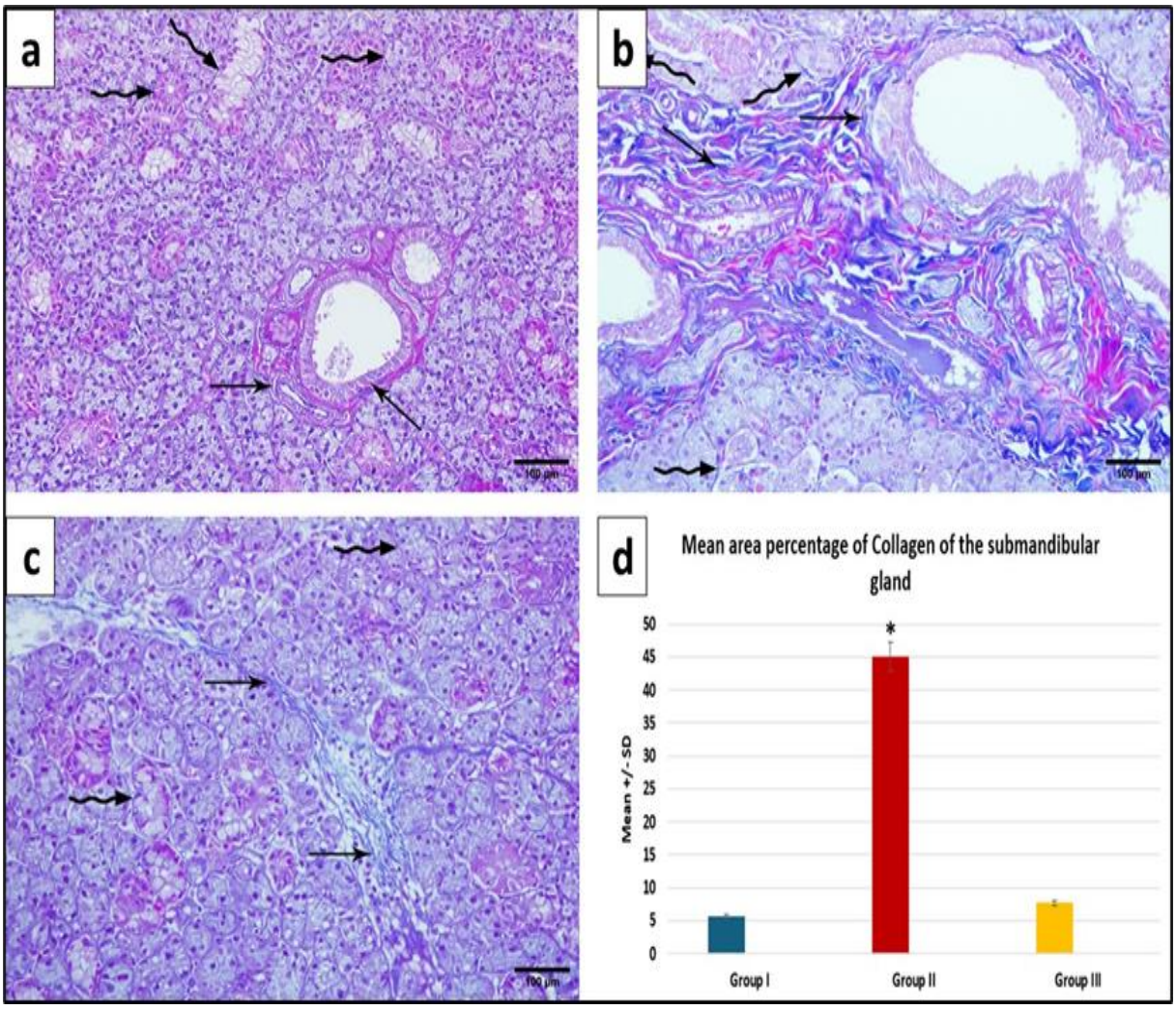

Fig. 5. Submandibular gland sections showing (a) control group (GI) shows fine scanty collagen fibers in the interlobular connective tissue surrounding the blood vessels and large excretory ducts (arrows) and around the intralobular ducts and acini (wavy arrows). (b) SOF-treated group (GII) shows an apparent marked deposition of collagen fibers in the interlobular connective tissue surrounding the blood vessels and excretory ducts (arrows) and around the intralobular ducts and acini (wavy arrows). (c) Withdrawal group (GIII) shows apparent moderate deposition of collagen fibers in the interlobular connective tissue (arrows) and around the intralobular ducts and acini (wavy arrows) (Masson's trichrome stained section, a, b and c x200 scale bar=100µ). (d) Mean area percentage of collagen in the submandibular gland of the different studied groups. The presented data are displayed by mean ± SD. * Highly significant difference of GII as compared to GI & GIII.

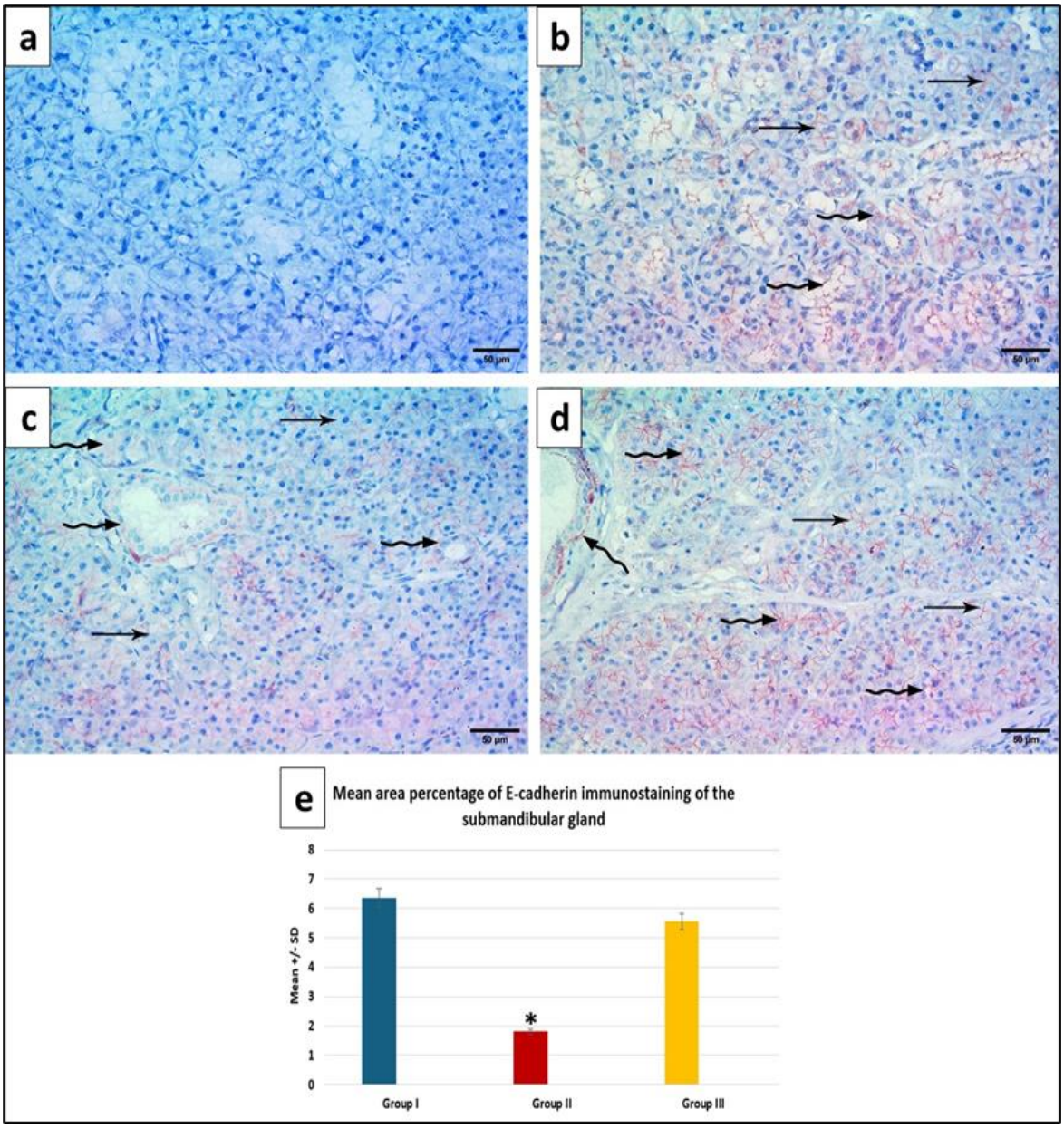

Fig. 6. Submandibular gland sections showing: (a) A negative control section. (b) Control group (GI) shows an apparent strong positive membranous reaction in the acini (arrows) and ducts (wavy arrows). (c) SOF-treated group (GII) shows an apparent weak positive membranous reaction in the majority of acini (arrows) and ducts (wavy arrows). (d) Withdrawal group (GIII) shows an apparent strong positive membranous reaction in the majority of acini (arrows) and ducts (wavy arrows) (a, b, c and d E-cadherin immunostaining x400 scale bar=50µ). (e) Mean area percentage of E-cadherin immunostaining in the submandibular gland of the different studied groups. The presented data are displayed by mean ± SD. * Highly significant difference of GII as compared to GI & GIII.

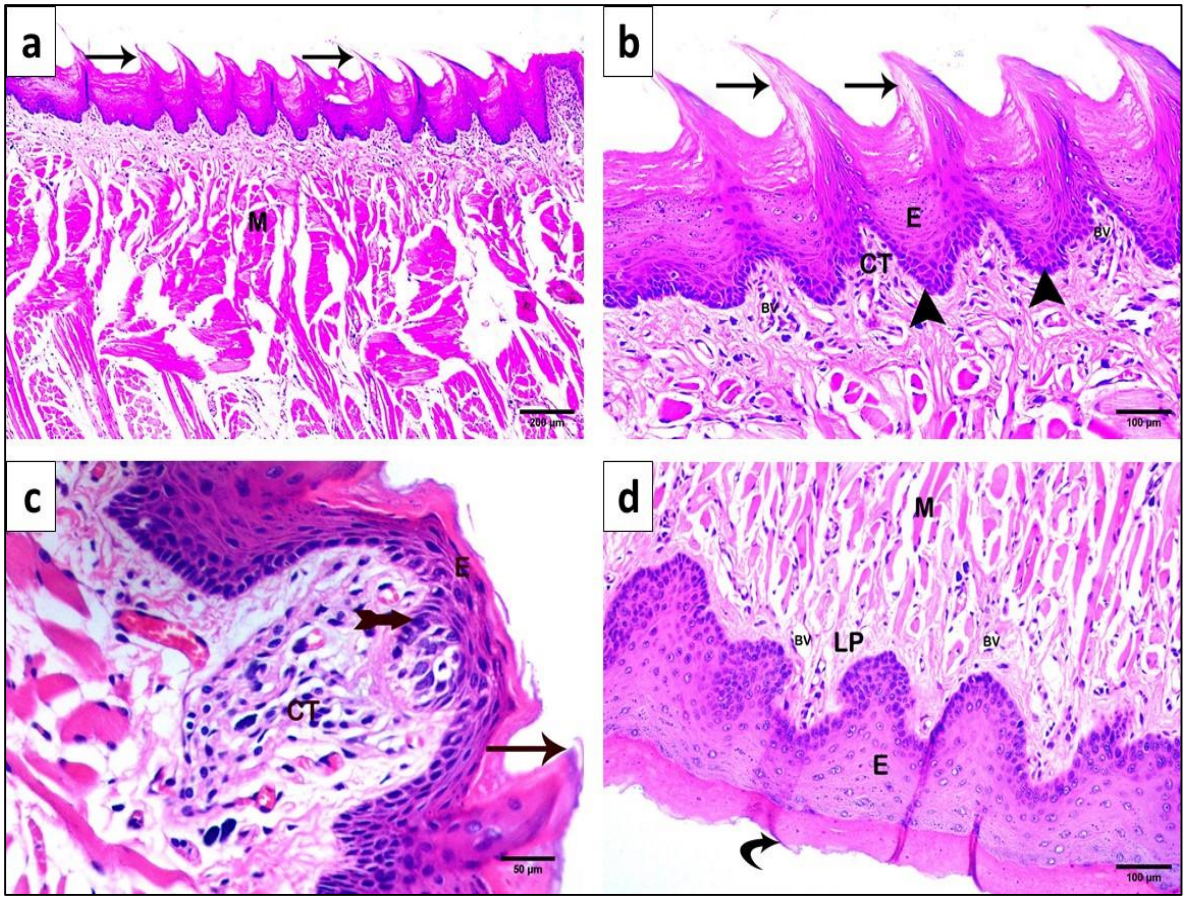

Fig. 7: Tongue sections of control group (GI) showing: (a, b) The dorsal surface of the tongue shows the normal distribution of the filiform papillae (arrows) which have characteristic sharp tapering ends. Each papilla is formed of a stratified squamous keratinized epithelium (E) resting on a basement membrane with ridges (arrow heads), and a connective tissue core (CT) with small blood vessels (BV). Lingual muscles (M) running in different directions are also observed. (c) A fungiform papilla in-between the filiform ones (arrow) that is covered by a stratified squamous epithelium keratinized (E) and has a connective tissue core (CT) is observed. A barrel taste bud (tailed arrow) in its upper surface is also seen. (d) The ventral surface shows the stratified squamous epithelium covering this surface (E) with a keratin layer (curved arrow) and the underlying lamina propria (LP) with small blood vessels (BV). Lingual muscles (M) are also observed. (H&E a x100 scale bar=200µ, b x200 scale bar =100µ, c x400 scale bar =50µ & d x200 scale bar =100µ).

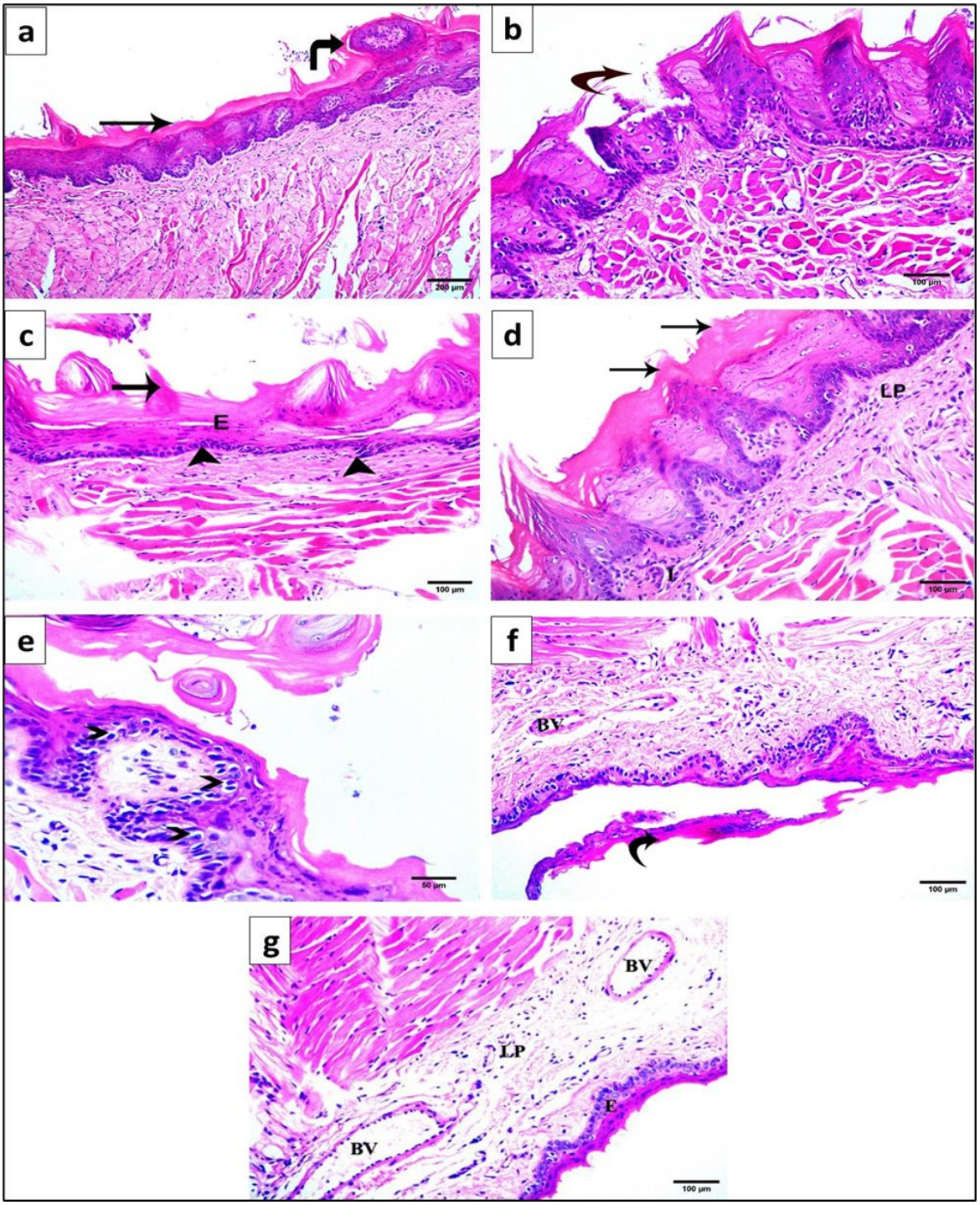

Fig. 8. Tongue sections of SOF-treated group (GII) showing: (a) The dorsal surface shows focal loss of the filiform papillae (arrows) and disorganized fungiform papillae (right-angled arrow). (b, c) Short filiform papillae (arrows) with focal discontinuity of the keratin layer (curved arrow). Apparent decrease in the epithelial layers (E) and absence of the papillary ridges (arrow heads) are also observed. (d) Short filiform papillae (arrows) and some appear with blunted end and inflammatory cellular infiltration (I) in the lamina propria (LP). (e) The covering epithelial cells show vacuolation of the cytoplasm and dark nuclei (➢). (f, g) The ventral surface shows focal separation of the layers within the epithelium (curved arrow) with apparent thinning of this covering epithelium (E). Dilatation of the blood vessels (BV) of the lamina propria (LP) is also noticed (H&E a x100 scale bar=200µ, b, c and d x200 scale bar =100µ, e x400 scale bar =50µ & f, g x200 scale bar =100µ).

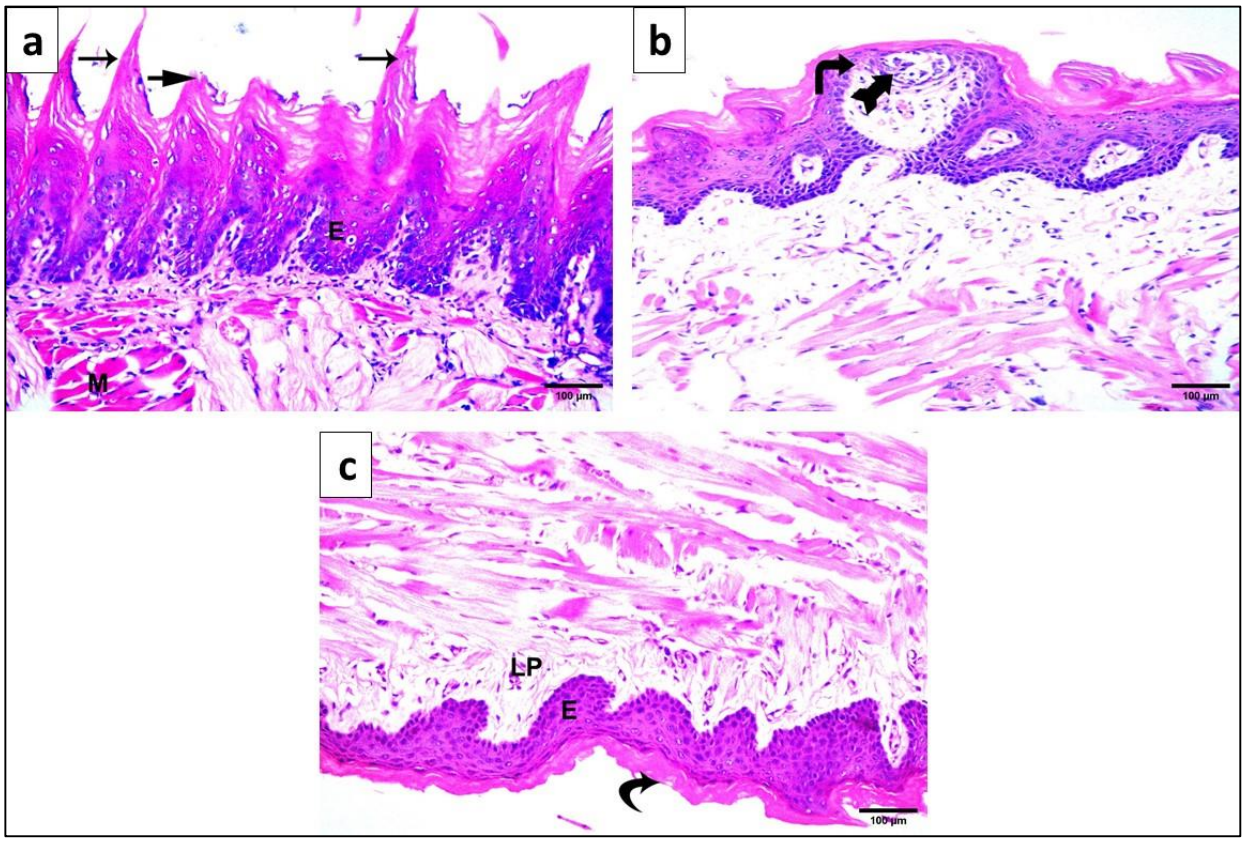

Fig. 9. Tongue sections of withdrawal group (GIII) showing: **(a, b)** The dorsal surface shows the regular shape of most filiform papillae (arrows). Few short, blunt papillae in- between them (short arrows) are noticed. Nearly normal epithelial covering (E) and ridges are also noticed. Nearly normal fungiform papilla (right-angled arrow) is noticed. A taste bud (tailed arrow) in its upper surface is also observed. Lingual muscles (M) run in different directions are seen. **(c)** The ventral surface of the tongue shows normal covering epithelium (E) with keratin layer (curved arrow) and normal lamina propria (LP) formed of loose CT **(**H&E a, b & c x200 scale bar=100µ**).**

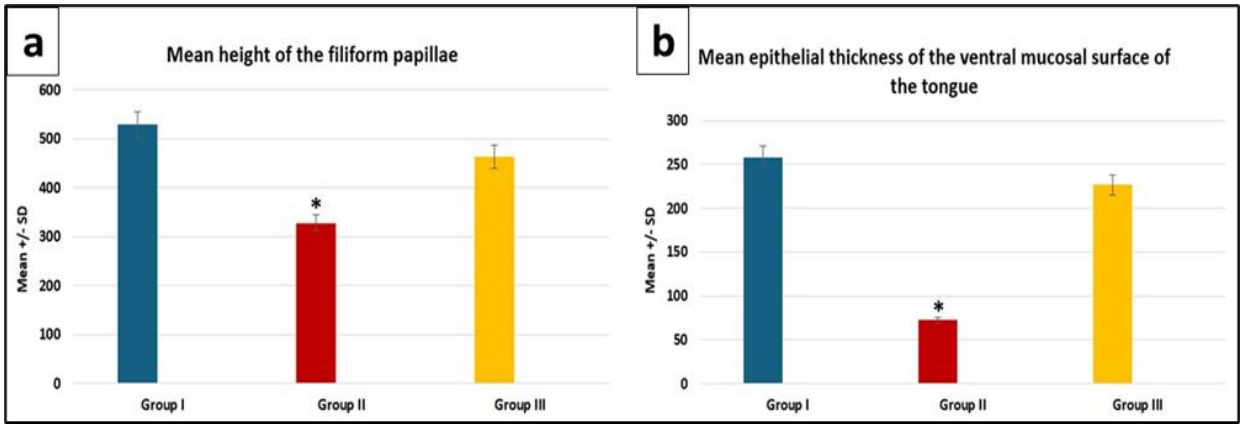

Fig. 10. Mean height of the filiform papillae **(a)** and mean epithelial thickness of the ventral mucosal surface of the tongue of the different studied groups **(b).** The presented data are displayed by mean ± SD. * Highly significant difference of group II as compared to groups I and III.

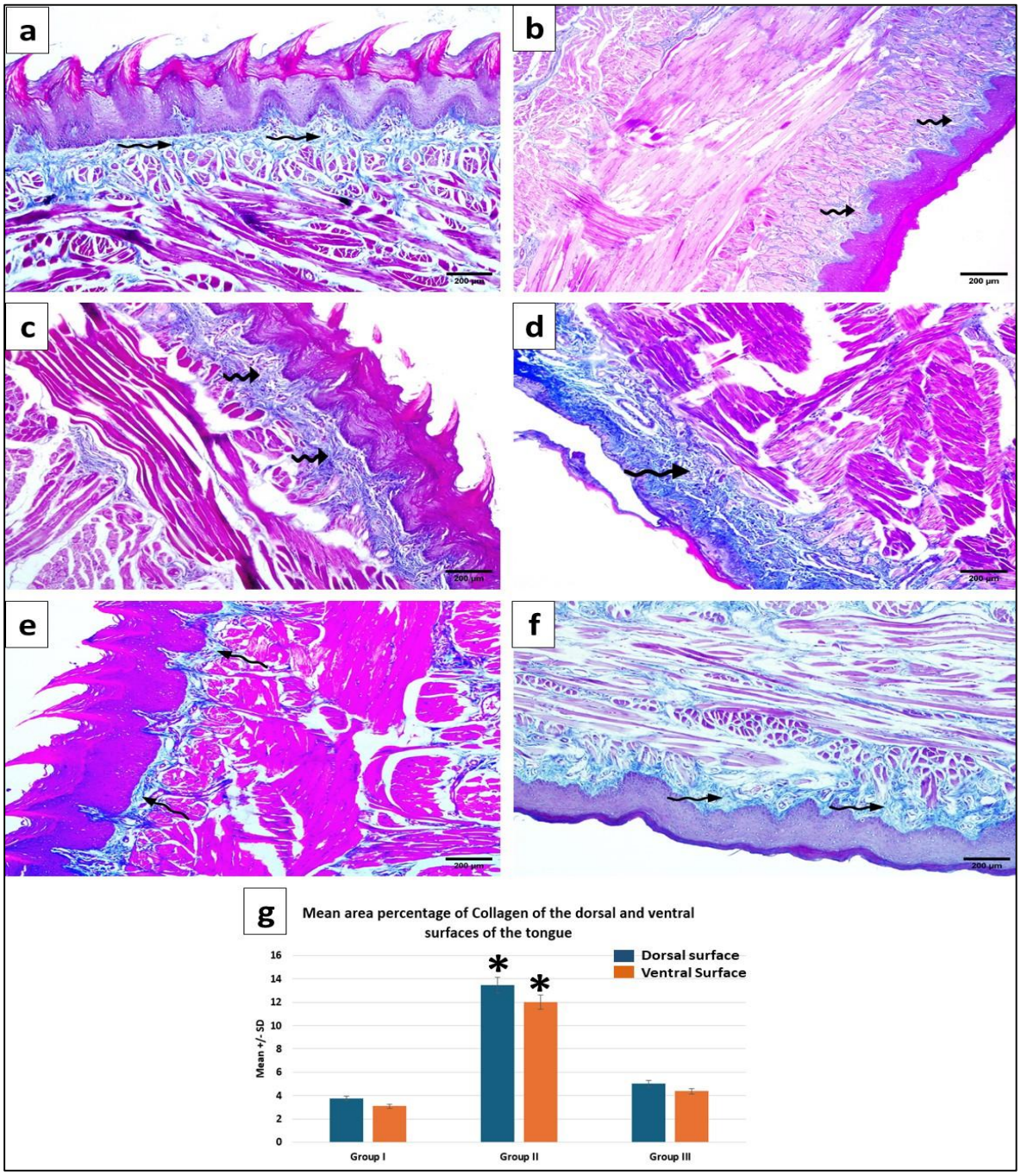

Fig. 11. Tongue sections showing: (a, b) the control group (GI) shows the dorsal and the ventral surfaces of the tongue, showing a sparse distribution of collagen fibers in the lamina propria (wavy arrows). (c, d) the SOF-treated group (GII) shows the dorsal and ventral surfaces of the tongue with apparent increase in collagen fiber deposition in the lamina propria (wavy arrows). **(e, f)** the withdrawal group (GIII) shows the dorsal and ventral surfaces of the tongue with a moderate distribution of collagen fiber in the lamina propria (wavy arrows) (Masson's trichrome; x100 scale bar=200µ). (g) Mean area percentage of collagen in the tongue of the different studied groups. The presented data are displayed by mean ± SD. * Highly significant difference of GII as compared to GI and GIII.

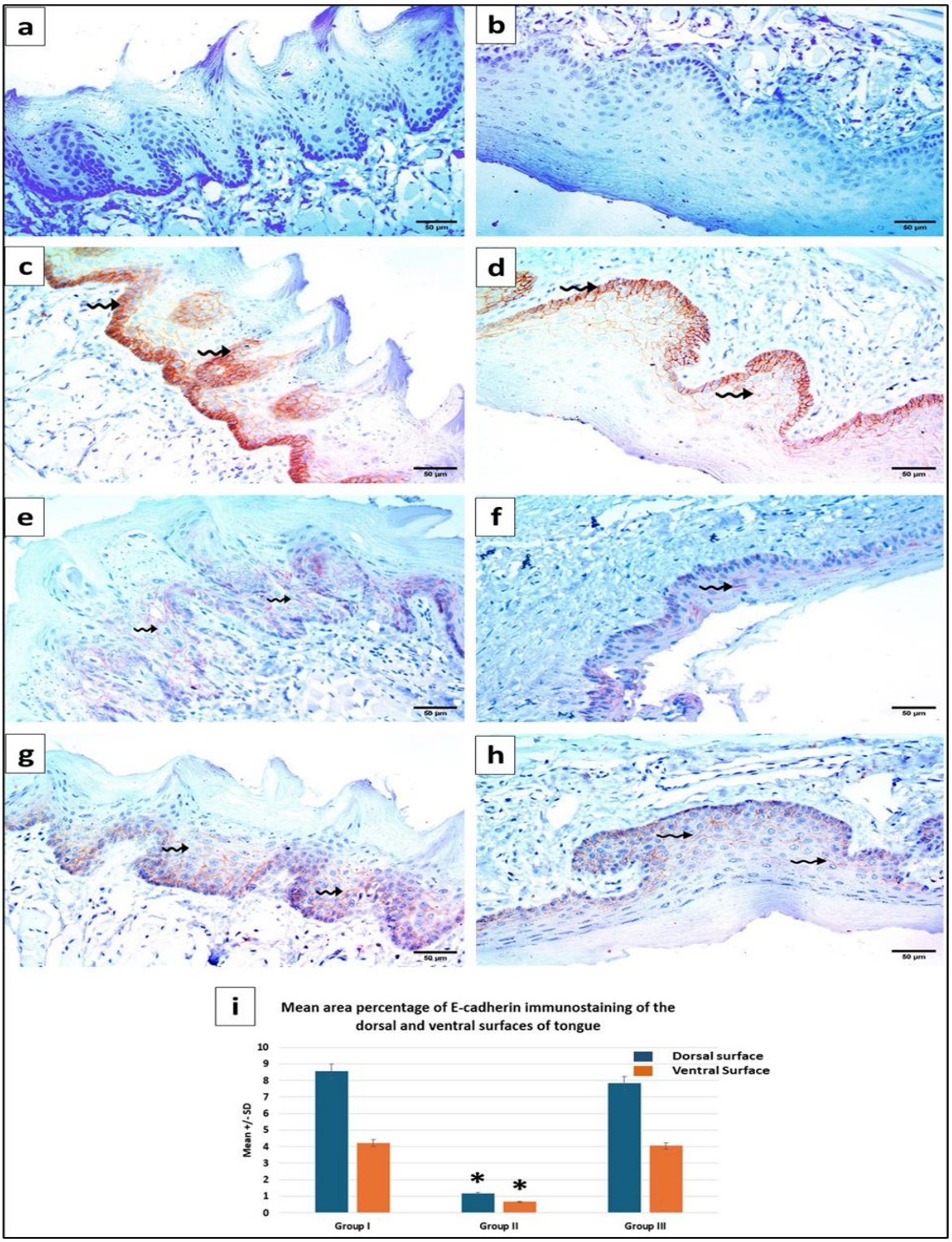

Fig. 12. Tongue sections showing: (a, b) Negative control sections of the dorsal and ventral surfaces respectively. (c, d) Control group (GI) shows the dorsal and ventral surfaces with an apparent strong positive membranous E-cadherin immunoreaction (wavy arrows) in nearly all epithelial layers. (e, f) SOF-treated group (GII) shows the dorsal and ventral surfaces with an apparent weak positive membranous E-cadherin immunoreaction in almost layers of the epithelium. (g, h) Withdrawal group (GIII) shows the dorsal and ventral surfaces with an apparent moderate positive membranous E-cadherin immunoreaction (wavy arrows) in nearly all epithelial layers (E-cadherin immunostaining a, b, c, d, e, f, g & h x400 scale bar=50µ). (i) Mean area percentage of E-cadherin immunostaining in the tongue of the different studied groups. The presented data are displayed by mean ± SD. * Highly significant difference of GII as compared to GI and GIII.

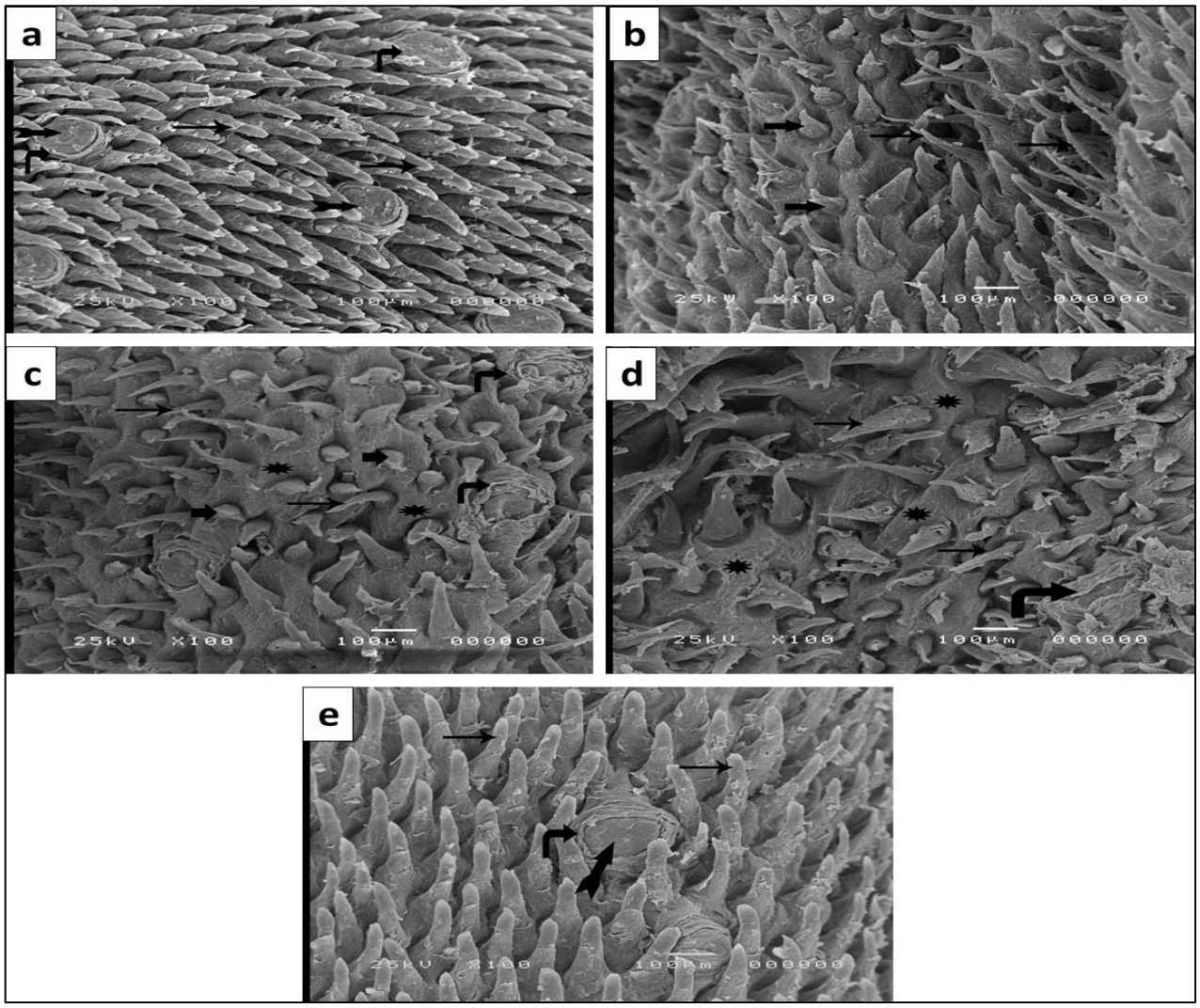

Fig. 13. Dorsal mucosal surface of tongue sections showing: (a) Control group (GI) shows numerous regularly arranged conical shaped filiform papillae (arrows) with tapering tips that directed in the same direction. Fungiform papillae (right angled arrow) having a taste pore (tailed arrows) in the center of its smooth surface are also noticed. **(b, c, d)** SOF-treated group (GII) shows irregularly arranged filiform papillae that run in different directions with wide spaces between them (Asterix). Some are thin and long (arrows) others are short and atrophied (thick arrows). Irregular fungiform papillae (right-angled arrow) with rough upper surface and ill-defined taste pore is also observed. **(e)** Withdrawal group (GIII) shows nearly normal filiform papillae (arrows) with scattered fungiform papilla (right-angled arrow) with taste pore (tailed arrow) in its center **(**SEM a, b, c, d & f x100 scale bar=100µ**).**

Discussion

Hepatitis C has been considered a core cause of hepatocellular carcinoma and liver failure (Aly et al., 2020). SOF has a potent antiviral efficacy, pangenotypic activity, advantageous pharmacokinetics, and superior tolerability and safety profile, it is regarded as the cornerstone of the majority of direct-acting antiviral combinations (Shawkat et al., 2022). The highly common side effects of SOF are mouth ulcers, and dry mouth (xerostomia) (Oakley, 2018; Khalil et al., 2023). Xerostomia with chronic salivary gland hypofunction can be diagnosed by a decreased number or even lost filiform papillae (Daniel et al., 2000), so, this study designed to demonstrate the impact of SOF and its withdrawal on the submandibular gland and the tongue of adult male albino rats. The results of this study displayed changes in the histological structure of both submandibular salivary gland and tongue in SOF-treated group (GII). Marked structural changes

affecting the submandibular gland lobules at both the acinar and ductal levels, thick interlobular connective tissue septa with evident fibrosis, infiltration of inflammatory cells and dilated congested blood vessels were prominent. The same findings were observed by Shawkat et al. (2022) who found widening of CT septa, blood vessel dilation and congestion, and inflammatory cellular infiltration. Also, Issa and El Sherif. (2017) previously exhibited the same findings, vascular dilatation and extravasation of blood within the neuropil in SOF treated group in addition to cellular infiltration within the cornea after 5 weeks of SOF administration. Mahran et al. (2022) also found that SOF treatment led to vascular congestion of the kidney. Congestion of blood vessels and inflammatory cellular infiltration could be explained by Mubarak (2012) and Asim et al. (2021) who mentioned that, in the case of a massive inflammation, a noteworthy break in the walls of the interstitial blood vessels leads to extravasation of red blood cells resulting in prevalent interstitial hemorrhages.

At the cellular level, the serous acinar cells showed various nuclear changes: fragmented, karyolitic and deeply stained pyknotic irregular nuclei with cytoplasmic vacuolations and diminished basophilia. This was in accordance with Mahmoud et al. (2020) who found time-dependent deterioration of the submandibular gland after SOF administration in the form of serous acini swelling with vacuolated cytoplasm. Pyknotic nuclei could be explained according to Sara et al. (2016) who reported that, elevated reactive oxygen species (ROS) caused mitochondrial disruption, which manifested as swelling and increased permeability in the mitochondria as well as an increase in caspase-3 production that led to apoptosis. Additionally, ROS raises pro-inflammatory cytokines, which activate caspase-3, a protein that limits both apoptosis and the inflammatory response (Refaie et al., 2017). Mahran et al. (2022) also linked the increase in the oxidative stress markers to SOF. The cytoplasmic vacuolation that was seen in this study could be explained by mitochondrial impairment, according to Miller and Zachary (2017), who noted that this could result in decreased ATP production, which would then deplete the Na-K pump and cause an accretion of water within the cells to control osmotic pressure. Additionally, Abdeen et al. (2019) linked the cytoplasmic vacuolization caused by SOF to mitochondrial toxicity. Concerning the intralobular ducts, the striated ducts showed cytoplasmic vacuoles and deeply stained nuclei, focal detachment of the basement membrane, and focal absence of the basal striations, in addition to stagnant secretion inside their lumina. The same findings were reported by Issa and El Sherif (2017a) who found some areas of apparent decrease and loss of corneal epithelium after 5 weeks of SOF administration. In addition, Salem et al. (2017) and Shawkat et al. (2022) confirmed the same results on the Eds excretory ducts of submandibular glands after SOF administration. Stagnant secretion could be explained by Buyuk et al. (2015) and El Ghusbi et al. (2014) documented that affected secretory protein production and disrupted secretory function in the submandibular salivary gland are the outcomes of oxidative stress. This secretory material consequently builds up in the acinar cells' cytoplasm, causing degeneration, cytoplasmic atrophy, nuclear changes, and even cell death. Concerning examination of the granular convoluted ducts lining cells revealed, vacuolated cytoplasm and deeply stained nuclei, widened intercellular spacing and sloughing of some cells into the lumina. The same findings were reported by Issa and El Sherif (2017a) and Shawkat et al. (2022) who revealed a widening of CT septa after 5 weeks of SOF treatment. These findings were similar to the findings of Salem et al. (2017) who mentioned that nuclear factor kappa b (NFkB) was clearly immune expressed when mitochondrial reactive oxygen species (mROS) were elevated, cellular vacuolization and deception in the basement membrane of some acini and granular convoluted ducts of their experimental groups as a result of SOF administration. Apparent changes in the histological structure of the tongue in SOF-treated group (G II) were evident. There was a disfigurement of the fungiform papillae.

Deterioration of the filiform papillae was evident by light microscope, scanning electron microscopic examination, morphometric, and statistical analysis. The same findings were observed by Khalil et al. (2023) and previously explained by Osman et al. (2006) who reported that filiform papillae have a high metabolic activity, along with sensitivity to enzymatic disruption, vascular insufficiency, and nutritional deficiencies. SOF-treated (GII) also depicted showed vacuolation of the cytoplasm and dark nuclei within the covering epithelial cells as well as a statistically significant decrease in the thickness of the epithelial layers. Statistically significant decrease in the length of filiform papillae along with inflammatory cellular infiltration in the CT core were also observed. The same observations were in accordance with Khalil et al. (2023), Feng et al. (2016) and Issa and Elsherif (2017a). According to Na et al. (2010), these alterations are caused by a disparity between ROS and antioxidants, which results in oxidative stress. Oxidative stress causes cellular death and hypoxia-mediated keratin intermediate filament disintegration and degradation.

Also, Mahmoud et al. (2023) detected that preconception exposure to SOF caused oxidative stress and disrupted normal cellular homeostasis in the liver, muscle, and placenta. They mentioned also that this inflammation was linked to a decline in total and reduced glutathione as well as an increase in oxidized glutathione and lipid peroxidation marker. It was reported that the hyposecretion of the submandibular gland, represented by the stagnant secretion in the lumina of ducts, could inversely affect the tongue papillae. This occurs mainly in the form of atrophy of the papillae (Togni et al., 2019). In addition, Erriu et al. (2016) reported that the drug- induced xerostomia could be a local factor for enhancement of the atrophy of tongue papillae. In this study, sections from the SOF-treated group (GII) revealed a significant rise in collagen fibers both in the submandibular gland and tongue versus the control group. This data was in the same line as Ali et al. (2024) who found increased collagen fibers in many organs in rats treated by SOF. Hosny et al. (2020) previously found a rise in the mean area percentage of myofibroblast α-smooth muscle actin (α-SMA) immunoreactivity in the SOF-treated group and revealed that SOF may have an impact on myofibroblast quantity and activity, which may lead to a buildup of collagen fibers. Helmers et al. (2015) supported that as they depicted that SOF could induce lung fibrosis. Regarding the immunohistochemical results, a significant decrease in E-cadherin immunoreactivity was detected in the SOF-treated group (GII) versus the control group in both submandibular gland and tongue. The same findings were detected by Hosny et al. (2020). The epithelium barrier's ability to function properly depends on the establishment of tight and adhesion junctions. Adherens junction, which contains the transmembrane protein E-cadherin, is crucial for the adhesion of epithelial cells and apical and basolateral polarization. It also suppresses the signaling pathways and regulates the proliferation and differentiation of epithelial cells (Tam et al., 2011; Nawijn et al., 2011).

Reduced packing and organization of the cells with compromised epithelial cell integrity is indicated by impaired E-cadherin expression (Post et al., 2018). Improvement and restoration of the histological structure in the submandibular gland and tongue in the withdrawal group (GIII) were apparent. In an attempt to explain this, it is documented that active myoepithelial cell proliferation occurs under chronic pathological settings; the proliferation activity indices are enhanced two-fold in the cells of the acini, four-fold in duct lining cells, and ten-fold in myoepithelial cells. Proliferation of the acini, ducts, and myoepithelial cells is essential for the regeneration of the salivary glandular structures as mentioned by Ihreler et al. (2004) and kujan et al. (2015). In conclusion, the discussed results verified that treatment with SOF has the potential to cause transient changes in submandibular gland and tongue histological structure which improves after its withdrawal.

Conflicts of interest

The authors assert no conflict of interest

References

Abdeen A M, Essawy T, Mohammed S S. Effect of sofosbuvir administration and its withdrawal on the submandibular salivary gland of adult male albino rats: A histological and ultra-structural study. *Open Access Macedonian Journal of Medical Sciences* (2019)*; 7*(23): 4101–4109.

Ali RA, Awadalla EA, Amin YA, Fouad SS, Ahmed MA, Hassan MH, Abdel-Kahaar E, Abdel-Aziz RH. The deleterious effects of sofosbuvir and ribavirin (antiviral drugs against hepatitis C virus) on different body systems in male albino rats regarding reproductive, hematological, biochemical, hepatic, and renal profiles and histopathological changes. Scientific Reports. 2024; 14:5682-5697.

Aly OA, Yousry WA, Teama NM, Shona EM, El Ghandour. Sofosbuvir and daclatasvir are safe and effective in treatment of recurrent hepatitis C virus in Egyptian patients underwent living donor liver transplantation. Egypt Liver Journal. (2020); 10(47).

Asim M, Ahmad F, Akhtar M. Florid interstitial hemorrhages: A novel feature of amoxicillin-clavulanate-induced acute tubulointerstitial nephritis. *The American Journal of Case Reports* (2021); *22*, e928989.

Bancroft JD and Layton C (2019a): hematoxylin and eosin. In: Suvarna S K, Layton CH and Bancroft JD Theory and Practice of Histological Techniques, 8th ed., Churchill Livingstone Elsevier, London. pp: 126-138.

Bancroft JD and Layton C (2019b): connective and other mesenchymal tissues with their stains. In: Suvarna S K, Layton CH and Bancroft JD Theory and Practice of Histological Techniques, 8th ed., Churchill Livingstone Elsevier, London. pp: 153-175.

Buyuk B, Parlak SN, Keles ON, Can I, Yetim Z, Toktay E et al. Effects of Diabetes on Post-Menopausal Rat Submandibular Glands: A Histopathological and Stereological Examination. Eurasian J Med 2015; 47(3): 199-207.

Cha A, Budovich A. Sofosbuvir: A New Oral Once-Daily Agent for The Treatment of Hepatitis C Virus Infection. Pharmacy &Theruputics 2014; 39(5): 345–352.

Daniels TE, Wu AJ. Xerostomia – Clinical Evaluation and Treatment in General Practice, Journal of the California Dental Association (2000); 28(12):933-941.

El- Gusbi GH, Shredah M, Soliman AB. Submandibular glands as an evident of the effects of antioxidant on alloxan-induced diabetic rats .World J Med Sci 2014; 11(2): 210-216.

El-ghazouly D EL, Yassien RI. Effect of Sofosbuvir (Sovaldi) on the Fundic Mucosa of Adult Male Albino Rats and the Possible Protective Role of Fucoidan: Histological, Histochemical, and Immunohistochemical Study. Egyptian Journal of histology. 2022; 45(1): 17-35.

El-Ghitany EM. Hepatitis C Virus Infection in Egypt: Current Situation and Future Perspective. Journal of high institute public health. 2019; 49(1):1-9.

Elkashef KA, Eman WA, Mesbah NM, Abo-Elmatty D M. Prevalence of Occult Hepatitis C Virus Infection in Egyptian Patients with Lymphoma: A New Vision. *Diagnostics*. 2022; *12*(4):10-15.

El-Kholy WB, Faried MA, Salama RM, El-Fiky MM, El-Garawani I. Evaluation of testicular cytotoxicity and genotoxicity of sofosbuvir and sofosbuvir - ribavirin in the adult male albino rats. Eur. J. Anat. 2019; 23 (6): 393-403.

Erriu, M., Pili, F. M., Cadoni, S., & Garau, V. (). Diagnosis of Lingual Atrophic Conditions: Associations with Local and Systemic Factors. A Descriptive Review. *The open dentistry journal* 2016; *10*: 619–635.

Essawy AS, Issa NM, Tayel SG. Glycyrrhiza Glabra Root Extract Alleviates Cyclophosphamide Induced Mucositis of the Tongue in Adult Male Albino Rats. ISSN 2021**;** 45(4): 1110-0559.

Feng J Y, Xu Y, Barauskas O, Perry J K, Ahmadyar S, Stepan G, Yu H et al . Role of mitochondrial RNA polymerase in the toxicity of nucleotide inhibitors of hepatitis C virus. *Antimicrobial Agents and Chemotherapy* (2016)*; 60*(2): 806–817.

Ghasi S, Umana I, Ogbonna A, Nwokike M and Ufelle S. Cradio protective effects of animal grade piperazine citrate on isoproterenol induced myocardial infarction in Wistar rats: Biochemical and histopathological evaluation.

African Journal of Pharmacy and Pharmacology. 2020; 14(8): 285-93.

Hassanin A, Kamel S, Waked I, and Fort M. Egypt's Ambitious Strategy to Eliminate Hepatitis C Virus: A Case Study. Glob Health Sci Pract. 2021; 9(1): 187–200.

Helmers RA, Byrne TJ, Wesselius LJ, Leslie KO. Serious Pulmonary Toxicity Secondary to Novel Hepatitis C Antiviral Therapy in a Liver Transplant Recipient. Mayo Clin Proc (2015); 90(9): 1294-1297.

Henriot p, Castry M, Nguyen LBL, Shimakawa Y, Jean K, Temime, L. Meta-analysis: risk of hepatitis C virus infection associated with hospital-based invasive procedures. Aliment Pharmacol Ther. 2022; 56(4):558-569.

Hosny S , Mohsen M A , Sabry M M.Histological study on the possible adverse effect of sofosbuvir on lungs of adult male albino rats.journal of medical histology(2020); 4(1):119-125.

Ibrahim EH, Elbealy MA, Nassar AA, Mostafa HM. Study of the effect of sofosbuvir based therapy on estimated glomerular filtration rate in Egyptian chronic hepatitis C patients. Journal of the Medical Research Institute 2021; 42(2): 7-13.

Ibrahim MAA, Sharaf Eldin HEM, Elswaidy NRM. Role of aqueous extract of saffron in ameliorating effect of sofosbuvir on the cerebellar cortex in rat. The Anatomical Record. 2020; 304(4): 673-913.

Ihrler S, Blasenbreu VS, Sendelhofert A, Rossle M, Harrison JD, Lohrs U. Regeneration in chronin sialadenitis: an analysis of proliferation and apoptosis based on double immunohistochemical labeling. Virchows Arch 2004; 444: 356-361.

Issa N M, El-Sherif N M. Light and electronic histological studies to the effect of Sofosbuvir on the visual cerebral cortex of adult male albino rat. Journal of American Science. (2017a) ;13(4).79-87

Issa N, El-Sherif N. Histological and Immunohistochemical Studies on the Cornea and Retina of Sofosbuvir Treated Rats. Austin J Anat. 2017b; 4(2):1068.

Kandeel, S, Elwan W. Effect of High Fat Diet on the Rat Submandibular Salivary Glands with the Possible Protection by Gomisin A: Light and Scanning Electron Microscopic Study. Egyptian Journal of Histology, 2023; 46(2): 588-602. doi: 10.21608/ejh.2022.100644.1576

Khalil F A Z, Abd El Hameed M M , El-Messiry H. The effect of antihepatitis c drug (sofosbuvir) on tongue papillae of albino rats and the possible modulatory action of grape seeds extract (histological and immunohistochemical study). Egyptian Dental Journal(2023); 69: 141-155.

Kujan O, Othman R, Alshehri M, Iqbal F, Kochaji N. Proliferative Activity of Myoepithelial Cells in Irradiated Rabbit Parotid and Submandibular Salivary Glands. J Int Oral Health 2015; 7(2):1-5.

Mahmoud A , Mohammed S , Essawy T. Histological and immunohistochemical evaluation to the effect of sofosbuvir administration on rat's submandibular salivary gland. Egyptian Dental Journal (2020); 4:575-583.

Mahmoud S A, Abdel-Aziz M M, Khafaga R HM, Hafez H A, Kamel M A, Shaker S A . The pre-conception maternal exposure to Sofosbuvir affects the mitochondrial biogenesis in prenatal fetal tissues. Experimental study on rats. *Mol Med* (2023); **29**: 71.

Mahran H, Okdah Y, Zaky A, Arisha S. The possible ameliorative role of Moringa oleifera seed oil on sofosbuvir-induced nephrotoxicity in albino rats; histopathological, immunohistochemical and biochemical studies. The Journal of Basic and Applied Zoology (2022); 83(16):2-12

Miller M A, Zachary J F (2017). Mechanisms and morphology of cellular injury, adaptation, and death. In J. F. Zachary & M. D. McGavin (Eds.), *Pathologic basis of veterinary disease* (6th ed.). Missouri: St Louis.

Mohamed AF, Abo-Ouf AM, Arafa MA. Histological and biochemical studies on effect of Sofosbuvir (Sovaldi) on adult male albino rat kidney. ultrastruct Pathol 2021; 45(4-5):286-296.

Mubarak R. Effect of red bull energy drink on rats submandibular salivary glands (light and electron microscopic study). Journal of American Science (2012); 8(1): 366-372.

Chandel N S, Litvan J, Ridge K M. Mitochondrial reactive oxygen species are required for hypoxia-induced degradation of keratin

intermediate filaments. The FASEB Journal (2010); 24(3): 799–809.

Nawijn MC, Hackett TL, Postma DS, Van Oosterhout AJ, Heijink IH. E-cadherin: gatekeeper of airway mucosa and allergic sensitization. Trends Immunol (2011); 32: 248–255.

Oakley, P. A. On the Side Effects of 'Pain' and 'Dehydration' in the Top 20 Selling Pharmaceuticals of 2017. Journal of Pharmaceutical Research International (2018); 21(6): 1–9.

Osman H I, EL Razek N, Koura A S. Histological changes of rat tongue papillae due to chromium toxicity and the protective role of vitamin E. Egyptian Dental Journal (2006);52: 193–200.

Post S, Heijink IH, Hesse L, Koo HK, Shaheen F, Fouadi M et al. Characterization of a lung epithelium specific E-cadherin knock-out model: Implications for obstructive lung pathology. Sci Rep (2018); 8: 13275.

Rau E, Gostev A, Shiqiu Z, Phang D, Chan D, Thong D, et al. Comparative analysis of scanning electron microscopy techniques for semiconductors: electron-beam-induced potential method, single-contact electron-beam-induced current method, and thermoacoustic detection. Russian Microelectronics. 2001;30(4):207-18.

Refaie M M, Ibrahim S A, Sadek S A, Abdelrahman A M. Role of ketotifen in methotrexate-induced nephrotoxicity in rats. *Egyptian Journal of Basic and Clinical Pharmacology* 2017*; 7*(2): 70–80

Salem Z A, Elbaz D A, Farag D B E. Effect of an Anti-Hepatitis C Viral Drug on Rat Submandibular Salivary Gland. Egyptian Dental Journal (2017); 63(1): 657-665.

Sara H, Rachid R, Gasmi S, Aml A, Amna A, Aya S et al . Oxidative stress status, caspase-3, stromal enzymes and mitochondria respiration and swelling of *Paramecium caudatum* in responding to the toxicity of Fe3O4nanoparticles. *Toxicology and Environmental Health Sciences (2016); 8*(2): 161–167.

Shalaby A, Kashef S, . The Effect of 5-Fluorouracil on the Tongue Mucosa of Adult Male Albino Rat and the Possible Protective Role of Melatonin: A Light and Scanning Electron Microscopic Study. *Egyptian Journal of Histology*, 2021; 44(3): 765-778.

Shawkat A , Ali Z , Bashir M. Histopathological Effect of Sofosbuvir as Compared to Sofosbuvir Combined with Ribavirin on Submandibular Salivary Glands of Adult Albino Rats (Histological and immunofluorescent study). Egyptian Journal of Histology (2022);46(3):1262-1271.

Sisto M, Ribatti D, Lisi S. E-Cadherin Signaling in Salivary Gland Development and Autoimmunity. J Clin Med. 2022 ;11(8):2241.

Tam A, Wadsworth S, Dorscheid D, Man SF, Sin DD. The airway epithelium: more than just a structural barrier. Ther. Adv. Respir. Dis (2011); 5: 255–273.

Togni L, Mascitti M, Santarelli A, Contaldo M, Romano A, Serpico R et al. Unusual Conditions Impairing Saliva Secretion: Developmental Anomalies of Salivary Glands. *Frontiers in physiology* 2019; *10*: 855.